Calculating Turbulent Reacting Flows Using Finite Chemical Kinetics

J. B. Vos*
Delft University of Technology, Delft, the Netherlands

A computer program that has been developed at the Delft University of Technology describing two-dimensional turbulent flows through channels with and without a sudden expansion was extended by accounting for heat and mass transfer at the boundaries. The wall-function method of Chieng and Launder was adapted allowing the calculation of the von Kármán constant E which is a function of the local boundary-layer structure in case of mass transfer. A finite chemical kinetics combustion model was implemented in this computer program. The equations for the mass fractions are solved in two steps. In the first step the convection and diffusion of mass fractions is taken into account. In the second step chemical reactions are taken into account by integrating the chemical source term using the integration method of Gear at each gridpoint in the flow domain. Results of calculations are presented.

Nomenclature

B	= constant in Arrhenius equation
$C_\ell, C_\mu, C_{\epsilon 1}, C_{\epsilon 2}$	= empirical constants in turbulence closure model
c_p	= specific heat at constant pressure
D	= diameter of the channel
E	= von Kármán constant
h	= enthalpy
h	= step height
k	= turbulent kinetic energy
L	= length of the channel
M	= molar mass
p	= static pressure
P_k	= production rate of turbulent kinetic energy
r	= coordinate
Re	= Reynolds number
R_0	= universal gas constant
S	= source term
T	= temperature
u	= velocity in x direction
V_j	= velocity vector
v	= velocity in r direction
v_w	= wall velocity
x	= coordinate
y	= distance from the wall
Y_s	= mass fraction
α	= constant in Arrhenius equation
Γ	= diffusion coefficient
ϵ	= dissipation rate of turbulent kinetic energy
κ	= von Kármán constant, = 0.42
μ_t	= turbulent viscosity
ν	= kinematic viscosity
ν	= stoichiometric coefficient
ρ	= density
$\sigma_t, \sigma_k, \sigma_\epsilon, \sigma_y$	= constants in turbulence closure model
τ	= shear stress
φ	= arbitrary variable
$\dot{\omega}_s$	= production or destruction rate

Subscripts

in	= inlet
k	= reaction
p	= point p
s	= species
t	= turbulent
v	= viscous sublayer
w	= wall

Superscripts

$()^+$	= normalized
$()''$	= Favre fluctuation
$()'$	= fluctuation
$(-)$	= mean
$()^a$	= reactants
$()^b$	= products

Presented as Paper 86-1655 at the AIAA/ASME/SAE/ASEE 22nd Joint Propulsion Conference, Huntsville, AL, June 16–18, 1986; received Aug. 25, 1986; revision received Jan. 23, 1987.

*Research Assistant, Faculty of Aerospace Engineering; currently Research Scientist, Swiss Federal Institute of Technology Lausanne, Institute of Fluid Mechanics, Lausanne, Switzerland.

Introduction

THE work described in this article deals with the theoretical investigation of the flow and combustion processes in solid fuel combustion chambers (SFCC's). An SFCC consists of a solid fuel grain with an inner bore. Air is fed into this bore, and at the interface between the pyrolizing solid fuel and the air, combustion will take place. Fuels which may be burnt in SFCC's are, for instance, waste materials and plastics such as polyethylene (PE) and polymethylmethacrylate (PMMA).

Seeking a better understanding of the flow and combustion processes in SFCC's, a joint research program is being conducted in the Netherlands by the Delft University of Technology and the Prins Maurits Laboratory TNO, Rijswijk. This research is both theoretical and experimental. An experimental facility was built allowing testing of SFCC's at pressures between 0.4 and 4 MPa, using inlet temperatures up to 1000 K. Spectroscopic diagnostic techniques are available to determine the local temperature and chemical composition within the burning gas. Experimental results of this research are presented in Ref. 1. In the first phase of the theoretical investigation of the flow and combustion processes in an SFCC, a computer program, called Computer Program for Parabolic and Elliptic Flows (COPPEF) was developed. COPPEF calculates two-dimensional steady turbulent flows in channels with and without a sudden expansion. Results of calculations carried out for the flow through a sudden expansion are discussed in Ref. 1. In the next two phases, the computer program was extended to account for

heat and mass transfer at the boundaries, and for combustion. Modeling of these processes is described and results of combustion calculations are presented, in which the pyrolizing solid fuel is simulated by a porous wall through which hydrogen is injected.

Governing Equations

The flow in an SFCC can be considered as highly turbulent. Typical Reynolds numbers based on the step height and inlet velocity are between 10^5 and 10^7. The wall of an SFCC consists of solid fuel that is pyrolized by a heat flux from the main flow to the wall. The pyrolizing fuel causes a mass flux of fuel from the wall to the main flow, where the fuel is burnt. At the entrance of the channel, a recirculation zone serves as a flame stabilizer, see Fig. 1. Obtaining a complete and detailed description of the flow and combustion processes in an SFCC is impossible because of the complex turbulence structures within the flow, and the poorly understood turbulence-chemistry interaction. Furthermore, the number of species and reactions involved in the combustion process is large, and little is known of many reactions. Careful simplifications have to be made to obtain a system of equations which can be solved numerically and which still describe the flow and combustion in an SFCC.

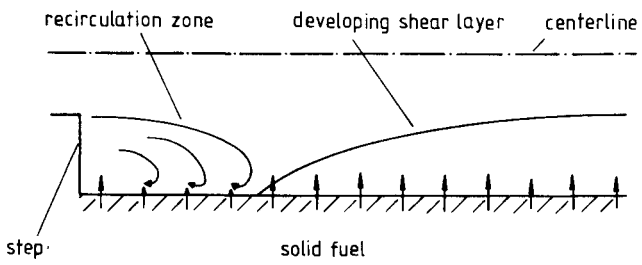

Fig. 1 The flow in a solid fuel combustion chamber.

The COPPEF computer program,[2] developed at the Delft University of Technology calculates two-dimensional turbulent flows through pipes with and without a sudden expansion. Turbulence is accounted for by Favre averaging of the conservation equations, and by modeling terms containing products of fluctuating variables with the high Reynolds number version of the k-ϵ turbulence closure model. All governing equations can be cast in the general form

$$\frac{\partial}{\partial x}(\rho u\varphi)+\frac{1}{r}\frac{\partial}{\partial r}(r\rho v\varphi)-\frac{\partial}{\partial x}\left(\Gamma_\varphi\frac{\partial\varphi}{\partial x}\right)-\frac{1}{r}\frac{\partial}{\partial r}\left(r\Gamma_\varphi\frac{\partial\varphi}{\partial r}\right)=S_\varphi \tag{1}$$

where φ, Γ_φ, and S_φ, together with the values of the turbulence closure model constants, are given in Table 1. The enthalpy h is defined as

$$h=\sum_s Y_s h_s \tag{2}$$

where Y_s is the mass fraction of species s and

$$h_s=h_s^0(T_0)+\int_{T_0}^{T} c_{p,s}\,\mathrm{d}T \tag{3}$$

h_s^0 is the enthalpy of species s at reference temperature T_0 and at standard conditions. The equation of state is written as

$$p=\rho R_0 T\sum_s\frac{Y_s}{M_s} \tag{4}$$

Table 1 Governing equation parameters

φ	Γ_φ	S_φ
1	0	0
u	μ_t	$-\frac{\partial p}{\partial x}-\frac{2}{3}\frac{\partial}{\partial x}(\mu_t\nabla\cdot V)-\frac{2}{3}\frac{\partial}{\partial x}(\rho k)+\frac{\partial}{\partial x}\left(\mu_t\frac{\partial u}{\partial x}\right)+\frac{1}{r}\frac{\partial}{\partial r}\left(r\mu_t\frac{\partial v}{\partial x}\right)$
v	μ_t	$-\frac{\partial p}{\partial r}-\frac{2}{3}\frac{1}{r}\frac{\partial}{\partial r}(r\mu_t\nabla\cdot V)-\frac{2}{3}\frac{1}{r}\frac{\partial}{\partial r}(r\rho k)+\frac{\partial}{\partial x}\left(\mu_t\frac{\partial u}{\partial r}\right)+\frac{1}{r}\frac{\partial}{\partial r}\left(r\mu_t\frac{\partial v}{\partial r}\right)-\frac{1}{r}\left[\mu_t\left(2\frac{v}{r}-\frac{2}{3}\nabla\cdot V\right)-\frac{2}{3}(\rho k)\right]$
h	μ_t	$-\frac{\partial}{\partial x}[\rho(u^2+v^2)]-\frac{1}{r}\frac{\partial}{\partial r}[r\rho(u^2+v^2)]+\left(\frac{1}{\sigma_t}-1\right)\left[\frac{\partial}{\partial x}\left(\mu_t\frac{\partial h}{\partial x}\right)+\frac{1}{r}\frac{\partial}{\partial r}\left(r\mu_t\frac{\partial h}{\partial r}\right)\right]$
k	$\frac{\mu_t}{\sigma_k}$	$P_k-\frac{\mu_t}{\rho^2\sigma_t}\left[\frac{\partial\rho}{\partial x}\frac{\partial p}{\partial x}+\frac{\partial\rho}{\partial r}\frac{\partial p}{\partial r}\right]-\rho\epsilon$
ϵ	$\frac{\mu_t}{\sigma_\epsilon}$	$C_{\epsilon_1}\frac{\epsilon}{k}\left[P_k-\frac{\mu_t}{\rho^2\sigma_t}\left(\frac{\partial\rho}{\partial x}\frac{\partial p}{\partial x}+\frac{\partial\rho}{\partial r}\frac{\partial p}{\partial r}\right)\right]-C_{\epsilon_2}\rho\epsilon^2/k$
Y_s	$\frac{\mu_t}{\sigma_y}$	$\dot\omega_s$

$$\nabla\cdot V=\frac{\partial u}{\partial x}+\frac{1}{r}\frac{\partial}{\partial r}rv;\qquad \mu_t=\rho C_\mu k^2/\epsilon$$

$$p_k=\mu_t\left\{2\left[\left(\frac{\partial u}{\partial x}\right)^2+\left(\frac{\partial v}{\partial r}\right)^2+\left(\frac{v}{r}\right)^2\right]+\left(\frac{\partial u}{\partial r}+\frac{\partial v}{\partial x}\right)^2\right\}-\frac{2}{3}(\rho k+\mu_t\nabla\cdot V)\left(\frac{\partial u}{\partial x}+\frac{1}{r}\frac{\partial rv}{\partial r}\right)$$

C_μ	C_{ϵ_1}	C_{ϵ_2}	C_ℓ	σ_t	σ_k	σ_ϵ	σ_y
0.09	1.44	1.92	2.56	0.7	1.0	1.3	0.7

The effect of density gradients on the turbulence field is taken into account by the pressure-velocity correlation term. This term occurs in the Favre-averaged equations for k and ϵ, and is written as

$$PV = -\overline{V_j''\frac{\partial p}{\partial x_j}} \simeq -\overline{V_j''}\frac{\partial \bar{p}}{\partial x_j} \tag{5}$$

The mean fluctuating velocity vector, which is not zero when Favre averaging is used, can be modeled as follows: from the definition of Favre averaging it follows that[3]

$$\overline{V_j''} = -\overline{\rho' V_j''}/\bar{\rho} \tag{6}$$

and the right-hand side of this equation may be modeled using an eddy-diffusivity concept

$$\bar{\rho}\overline{V_j''\rho'} = -\frac{\mu_t}{\sigma_t}\frac{\partial \bar{\rho}}{\partial x_j}$$

The pressure-velocity correlation term finally yields

$$PV = -\frac{\mu_t}{\sigma_t}\frac{1}{\bar{\rho}^2}\frac{\partial \bar{p}}{\partial x_j}\frac{\partial \bar{\rho}}{\partial x_j} \tag{7}$$

As can be seen from Eq. (7), density gradients can generate turbulence, but they can also suppress it.

Boundary Conditions

The partial differential equations [Eq. (1)] can be solved if the required boundary conditions are specified. Inlet conditions specified are

$$u = u_{\text{in}}, \quad v = 0, \quad k = 0.005u_{\text{in}}^2$$

$$\epsilon = 0.09k^{3/2}/(0.03r_{\text{in}})$$

$$p = p_{\text{in}}, \quad h = c_p T_{\text{in}}, \quad Y_s = (Y_s)_{\text{in}}$$

At the outlet and the centerline of the channel, a no-gradient condition is used for all equations except the r-momentum equation for which a zero velocity is specified,

$$\text{outlet:} \quad \frac{\partial \varphi}{\partial x} = 0 \qquad v = 0$$

$$\text{centerline:} \quad \frac{\partial \varphi}{\partial r} = 0 \qquad v = 0$$

At solid walls, the following conditions are specified

$$u = 0, \quad v = 0 \text{ or } v = v_w, \quad T = T_w, \quad Y_s = (Y_s)_w$$

The values of k and ϵ are not specified at the wall, but are calculated just near the wall using wall functions. Near solid walls, viscous effects become important due to the no-slip condition at the wall. The k-ϵ model in the form incorporated in COPPEF is valid only for high-Reynolds-number flows. To account for viscous or low-Reynolds number effects near solid walls the production and dissipation terms in the equations for k and ϵ are replaced by expressions obtained from wall-functions. The two-layer wall function method of Chieng and Launder[4] is incorporated in the COPPEF computer program. A distinction has to be made between walls with and without blowing or suction. In principle, wall functions cannot be used in flows with blowing or suction. As the regression rates of most solid fuels are very small, blowing velocities are small (<0.1 m/s) and the boundary layer will only be slightly affected. An adapted version of the wall-function method of Chieng and Launder is developed that is used in flows with blowing or suction.

For an impermeable wall, the wall-function method of Chieng and Launder is summarized as follows. It is assumed that the boundary layer near a solid wall can be divided into two regions, a viscous sublayer close to the wall, and a fully turbulent region, see Fig. 2a. The interface between the viscous sublayer and the fully turbulent region is taken such that $Re_v = k_v^{1/2} y_v/\nu$ equals 20. The velocity component parallel to the wall is assumed to vary with the distance to the wall according to

$$u = \frac{\tau_w}{\rho k_v^{1/2}\kappa C_\mu^{1/4}} \ln(E y k_v^{1/2} C_\mu^{1/4}/\nu) \tag{8}$$

where $\kappa(=0.42)$ and $E(=9.0)$ are the von Kármán constants. Shown in Fig. 2b, the turbulent kinetic energy in the near-wall cell is assumed to vary parabolically near the wall and linearly in the fully turbulent region

$$k = (y/y_v)^2 k_v \qquad 0 \le y < y_v \tag{9a}$$

$$k = ay + b \qquad y_v \le y \le y_e \tag{9b}$$

where $a = (k_E - k_p)/(y_E - y_p)$ and $b = k_p - a y_p$.

The turbulent kinetic energy at the edge of the viscous sublayer, and the viscous sublayer thickness can be solved from Eq. (9) and the definition of Re_v. As shown in Fig. 2c, the turbulent shear stress is zero in the viscous sublayer, and increases abruptly at the edge of the viscous sublayer. In the fully turbulent region, it is assumed that the turbulent shear stress varies linearly with the distance to the wall, i.e.,

$$\tau_t = 0 \qquad 0 \le y < y_v \tag{10a}$$

$$\tau_t = \tau_w + (\tau_e - \tau_w) y/y_e \qquad y_v \le y \le y_e \tag{10b}$$

The dissipation rate ϵ in the viscous sublayer is a constant equal to

$$\epsilon = 2\nu\left(\frac{\partial k^{1/2}}{\partial y}\right)^2 = 2\nu k_v/y_v^2 \qquad 0 \le y < y_v \tag{11a}$$

while in the fully turbulent region, ϵ can be approximated by

$$\epsilon = k^{3/2}/C_\ell y \tag{11b}$$

The mean production rate of turbulent kinetic energy P_k, may in the near-wall cell be calculated from

$$P_k = \frac{1}{y_e}\int_{y_v}^{y_e} \tau_t\left(\frac{\partial u}{\partial y} + \frac{\partial v}{\partial x}\right) dy$$

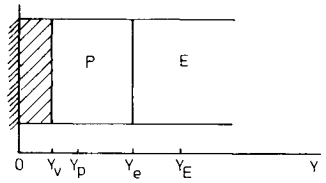

a) Near-wall cell.

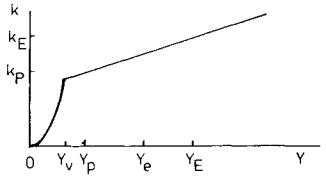

b) Assumed turbulent kinetic energy distribution.

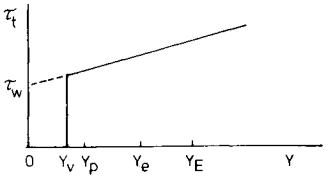

c) Assumed turbulent shear stress distribution.

Fig. 2 Near-wall model wall functions.

Integrating this equation using Eqs. (8-10) yields

$$P_k=\frac{\tau_w(u_e-u_v)}{y_e}+\frac{\tau_w(\tau_e-\tau_w)}{\rho\kappa C_\mu^{1/4}k_v^{1/2}y_e}\left(1-\frac{y_v}{y_e}\right)$$
$$+\left\{\tau_w\left(1-\frac{y_v}{y_e}\right)+\frac{\tau_e-\tau_w}{2}\left[1-\left(\frac{y_v}{y_e}\right)^2\right]\right\}\frac{\partial v}{\partial x} \qquad (12)$$

The mean dissipation rate in the k equation is calculated from

$$\epsilon=\frac{1}{y_e}\int_0^{y_e}\epsilon dy=\frac{2k_v^{3/2}}{y_eRe_v}+\frac{1}{y_eC_\ell}\left[\frac{2}{3}(k_e^{3/2}-k_v^{3/2})\right.$$
$$\left.+2b(k_e^{1/2}-k_v^{1/2})+|b|^{3/2}\lambda\right] \qquad (13)$$

where

$$\lambda=\ell n\left[\frac{(k_e^{1/2}-b^{1/2})(k_v^{1/2}+b^{1/2})}{(k_v^{1/2}-b^{1/2})(k_e^{1/2}+b^{1/2})}\right] \qquad \text{if } b>0$$
$$=2\left[\tan^{-1}\left(\frac{k_e}{-b}\right)^{1/2}-\tan^{-1}\left(\frac{k_v}{-b}\right)^{1/2}\right] \qquad \text{if } b<0$$

Equations (12) and (13) replace the production and dissipation terms in the transport equation for the turbulent kinetic energy in the near-wall cell. The dissipation rate ϵ in the near-wall cell is calculated from Eq. (11b)

$$\epsilon_p=k_p^{3/2}/C_\ell y_p \qquad (14)$$

This corresponds with the assumption of a universal dissipation length scale $\ell=C_\mu^{-3/4}\kappa y=C_\ell y$ in the near-wall region.

The link between the near-wall variation of the temperature and the heat flux to the wall is given by

$$\frac{\rho c_p(T_w-T)k_v^{1/2}}{q_w''}=\sigma_t\left(\frac{uk_v^{1/2}}{\tau_w/\rho}+C_\mu^{-1/4}P\right) \qquad (15)$$

where P is the Jayatilleke function[5]

$$P=9.0[(\sigma/\sigma_t)^{0.75}-1]\cdot[1+0.28\exp(-0.007\sigma/\sigma_t)] \qquad (16)$$

In the case of a wall with blowing or suction, the wall-function method of Chieng and Launder has to be adapted to account for a normal velocity at the wall. Analogous to the method for an impermeable wall, it is assumed that the boundary layer can be divided into a viscous sublayer and a fully turbulent region (see Fig. 2a), where the edge of the viscous sublayer is located at $Re_v=20$. From a Couette flow analysis, it is found that the velocity component parallel to the wall in the case of blowing or suction in the fully turbulent region varies as[6]

$$\frac{uC_\mu^{1/4}k_v^{1/2}}{\tau_w/\rho}=\frac{\ell n(EC_\mu^{1/4}k_v^{1/2}y/\nu)}{\kappa}+\frac{v_wC_\mu^{1/4}k_v^{1/2}}{\tau_w/\rho}\left[\frac{\ell n(EC_\mu^{1/4}k_v^{1/2}y/\nu}{2\kappa}\right]^2 \qquad (17)$$

The von Kármán constant E is no longer a constant, but depends on the local flow and boundary-layer structure. From Eq. (17) it follows that the wall shear stress can be calculated from

$$\tau_w=\rho C_\mu^{1/4}k_v^{1/2}\left[\frac{\kappa u}{\ell n(EC_\mu^{1/4}k_v^{1/2}y/\nu)}-\frac{v_w}{4\kappa}\ell n(EC_\mu^{1/4}k_v^{1/2}y/\nu)\right] \qquad (18)$$

The von Kármán constant E is calculated as follows. From Eq. (9) and the definition of Re_v, it is possible to calculate y_v and k_v. Substitution of the velocity at the near-wall gridpoint u_p and the distance from the near-wall gridpoint to the wall y_p into Eq. (18), results in an equation with two unknowns, τ_w and E. In the viscous sublayer, the shear stress distribution in the case of blowing or suction is given by[6]

$$\tau=\mu\frac{du}{dy}=\tau_w+\rho v_wu \qquad 0\le y<y_v \qquad (19)$$

At the edge of the viscous sublayer, this equation may be approximated to yield

$$\mu(u_v/y_v)=\tau_w+\rho v_wu_v \qquad (20)$$

which is also an equation with two unknowns, τ_w and u_v. Substitution of y_v into Eq. (18) yields an equation with three unknowns, τ_w, u_v, and E; and a system of three equations with three unknowns, τ_w, u_v, and E, is formed which can be solved.

The production rate of turbulent kinetic energy is, in the case of blowing or suction, calculated from

$$P_k=\frac{1}{y_e}\int_{y_v}^{y_e}\left[\tau_w+(\tau_e-\tau_w)\frac{y}{y_e}\right]\left(\frac{\partial u}{\partial y}+\frac{\partial v}{\partial x}\right)dy \qquad (21)$$

From Eq. (17), it follows that

$$\frac{\partial u}{\partial y}=\frac{\tau_w}{\rho k_v^{1/2}\kappa C_\mu^{1/4}y}+\frac{v_w}{4\kappa^2}\frac{2}{y}\ell n(EC_\mu^{1/4}yk_v^{1/2}/\nu) \qquad (22)$$

Substitution of Eq. (22) into Eq. (21) and subsequent integration yields

$$P_k=\frac{\tau_w(u_e-u_v)}{y_e}+\frac{\tau_w(\tau_e-\tau_w)}{\rho\kappa C_\mu^{1/4}k_v^{1/2}y_e}\left(1-\frac{y_v}{y_e}\right)$$
$$+\left\{\tau_w\left(1-\frac{y_v}{y_e}\right)+\frac{(\tau_e-\tau_w)}{2}\left[1-\left(\frac{y_v}{y_e}\right)^2\right]\right\}\frac{\partial v}{\partial x}$$
$$+\frac{v_w}{2\kappa^2}\left(\frac{\tau_e-\tau_w}{y_e}\right)\times\left\{\ell n(EC_\mu^{1/4}k_v^{1/2}y_e/\nu)-1\right.$$
$$\left.-\frac{y_v}{y_e}[\ell n(EC_\mu^{1/4}Re_v)-1]\right\} \qquad (23)$$

The last term of this equation is the contribution of a non-zero normal velocity at the wall to the production rate of turbulent kinetic energy. In the case of blowing, the production rate of turbulent kinetic energy is increased; in the case of suction, the turbulence level is reduced. The mean dissipation rate of turbulent kinetic energy is, in the case of blowing or suction, calculated from Eq. (13). The dissipation rate itself in the near-wall gridpoint is calculated from Eq. (14). The heat flux to the wall is, in the case of blowing or suction, calculated from[6]

$$\frac{\rho c_p(T_w-T)k_v^{1/2}C_\mu^{1/4}}{q_w''}=\left[\left(1+\frac{v_wu_p}{\tau_w/\rho}\right)^{\sigma_t}\right.$$
$$\left.\times\exp\left(\frac{\sigma_tv_wP}{k_v^{1/2}C_\mu^{1/4}}\right)-1\right]\Big/\frac{v_w}{k_v^{1/2}C_\mu^{1/4}} \qquad (24)$$

where P is the Jayatilleke function [Eq. (16)].

Combustion Modeling

During the last 15-20 years much attention has been given to the modeling of flows with combustion, although a detailed prediction of turbulent flows with combustion still cannot be made for two reasons. First, the number of species

and reactions involved in even a simple combustion process, for instance the formation of water, is large, requiring the solution of large systems of strongly coupled equations at every gridpoint in the flowfield. For combustion processes involving complex hydrocarbons, the number of species and reactions involved is tremendously large, and even the most powerful computers of today are not able to solve this problem. Little is known of one complication, that of many reactions, especially reactions involving complex hydrocarbons. Second, in turbulent flows, turbulent fluctuations affect the combustion process. Because the chemical production/destruction rate is a nonlinear function of the mass fractions and the temperature, the determination of the mean chemical production/destruction rate is extremely difficult and requires the modeling of a large number of terms containing products of fluctuating variables. Many combustion models available today attempt to get around the evaluation of the mean chemical production/destruction rate. For instance, within the diffusion flame concept it is assumed that chemical reaction rates are so fast that fuel and oxidizer cannot exist together at the same place and time. The mixing of fuel and oxidizer is the flame-controlling mechanism, and it can be shown[7] that the mixture composition and thermochemical state may be related to one conserved scalar. However, within this concept it is impossible to predict the combustion process in an SFCC in detail, because only one irreversible reaction of the form fuel + oxidizer = products is considered. Within the framework of the SFCC project, spectroscopic means are available to determine the instantaneous temperature and mixture composition. From these data information about species and reactions involved in the combustion process can be obtained. The combustion model selected to be incorporated in the COPPEF computer program must therefore be able to account for several reactions and species, including the formation of pollutants, for instance carbon monoxide (CO) and nitrogen oxides (NO_x). Only a combustion model based on finite chemical kinetics satisfies these requirements, and is therefore implemented in COPPEF. The influence of turbulent fluctuations on the combustion process is, at this stage, neglected.

The finite chemical kinetics combustion model can be summarized as follows. Consider the general system of opposing chemical reactions

$$\sum_s \nu^a_{s,k} A_s \underset{k_{f,k}}{\overset{k_{b,k}}{\rightleftharpoons}} \sum_s \nu^b_{s,k} A_s, \qquad k = 1,\ldots,m \tag{25}$$

where A_s denotes the chemical symbol for species s, and $k_{f,k}$ and $k_{b,k}$ the forward and backward reaction rates, respectively. The mean chemical production/destruction rate of species s, $\dot{\omega}_s$, can be calculated from[8]

$$\dot{\omega}_s = M_s \sum_k (\nu^b_{s,k} - \nu^a_{s,k}) k_{f,k} \rho^{m_1} \Pi_s \left(\frac{Y_s}{M_s}\right)^{\nu^a_{s,k}} \times \left[1 - \frac{1}{K_{c,k}} \rho^{m_2} \Pi_s \left(\frac{Y_s}{M_s}\right)^{(\nu^b_{s,k} - \nu^a_{s,k})}\right] \tag{26}$$

where

$$m_1 = \sum_s \nu^a_{s,k} \qquad m_2 = \sum_s (\nu^b_{s,k} - \nu^a_{s,k})$$

The forward reaction rate constant is calculated from an Arrhenius expression

$$k_{f,k} = B_k T^{\alpha_k} e^{-E_k/T} \tag{27}$$

where B_k and α_k are constants, and E_k the activation energy. The equilibrium constant $K_{c,k}$, defined as the ratio of forward and backward reaction rate constants, is calculated from

$$K_{c,k} = (R^* T)^{-m_2} \exp\left[\left(\sum_s \nu^a_s F^0_s - \sum_s \nu^b_s F^0_s\right) \Big/ (RT)\right] \tag{28}$$

where R^* is the universal gas constant divided by one atmosphere ($= 1.01325 \times 10^5$ N/m^2) and F^0_s the Gibbs free energy for species s.

Solution Procedure

The general partial-differential equation [Eq. (1)] is integrated over a small control volume to obtain an algebraic difference equation that can be solved numerically. This method ensures that over the control volume the conservation equations are always satisfied. The dimensions of the control volumes may be chosen arbitrarily. Small control volumes are used in regions where variables contain large gradients whereas in other regions larger control volumes are sufficient for an accurate approximation of the variables. A staggered grid system is used in which the u and v velocities are stored at the boundaries of the control volume for the other variables. When calculating the convective fluxes across the control volume interfaces, the velocities are directly available. Moreover, when solving the momentum equations, the pressure difference between two adjacent gridpoints becomes the driving force of the velocity component located between these gridpoints. The total flux (convective plus diffusive) across the control volume boundary is approximated by the Power-law scheme.[9]

Solving the system of equations simultaneously requires the formation and solution of large systems of matrices, which are extremely expensive to compute. Therefore, a segregated solution approach is adopted, in which each variable is solved from an algebraic difference equation. An iteration procedure is used to account for the nonlinear coupling. However, this segregated approach leads to problems with the coupling between the pressure and velocity field. If the correct pressure field is substituted into the momentum equations, the resulting velocity field must satisfy the continuity equation. To account for this coupling, the Semi-Implicit Method for Pressure Linked Equations Revised (SIMPLER) procedure[9] is used. In SIMPLER the pressure p and a pressure correction p' are calculated from the continuity equation. The pressure is substituted into the momentum equations to calculate the axial and radial velocities, and the pressure correction is used to correct these velocities to satisfy the continuity equation. Besides the SIMPLER algorithm a line continuity correction method is incorporated in COPPEF. This procedure adjusts the u velocity and pressure field to ensure that at every gridline overall continuity is satisfied. When solving the algebraic difference equation for the pressure correction equation, a block correction procedure[10] is employed to ensure that the residual of this equation goes to zero.

The equations for the mass fractions are treated in a different manner, because the source-dominated character of these equations prohibits solution with the standard solution approach. The chemical source term is much larger than the convection and diffusion terms, and the mass-fraction equations can only be solved if the maximum allowable change in Y_s in one iteration cycle is strongly limited to ensure that $Y_s \geq 0$ and $Y_s \leq 1$. This results in a tremendous number of iterations required to solve the system of equations. Solving the mass fraction equations is therefore split into two steps. In the first step, convection and diffusion of mass fractions is accounted for using the standard solution procedure incorporated in COPPEF. In the second step, chemical reactions are taken into account for all mass fractions simultaneously by solving

$$\frac{\mathrm{d}}{\mathrm{d}t}(\rho Y_s) = \dot{\omega}_s \tag{29}$$

for each control volume, where the integration time is related to the residence time of the gas in the control volume. The two steps in this pseudo-time-splitting algorithm are connected together by the overall iteration procedure. Equation (29) is solved by means of the integration procedure suitable for stiff ordinary-differential equations developed by Gear.[11] The solution procedure can be summarized as:

1) Guess the velocity field.
2) Calculate pressure p.
3) Calculate u and v.
4) Correct u and p to satisfy overall continuity.
5) Calculate p', and correct u and v satisfy cell continuity.
6) Calculate h, k, ϵ.
7) Account for convection and diffusion of Y_s.
8) Solve Eq. (29) at every gridpoint.
9) Return to step 1 until convergence is reached.

Calculation Results

The adapted wall-function method of Chieng and Launder was used for the calculation of a flow without combustion through a pipe with a sudden expansion, with injection of mass at the wall. Calculations were carried out using a 20×20 grid system for a flow with a Reynolds number of 72,000. The inlet velocity was equal to 30 m/s, and the expansion ratio of the channel equal to 0.5. The injected gas and the gas in the inlet stream were equal. The calculated values of the von Kármán constant E for different blowing velocities are shown in Fig. 3. Calculated reattachment lengths varied between 7.98 step heights for the calculation made with $v_{inj} = 0.025$ m/s up to 8.28 step heights for the calculation with $v_{inj} = -0.01$ m/s. It may be seen from Fig. 3 that the behavior of the calculated von Kármán constant in the recirculation region is different from the behavior in the developing shear layer region. In the latter region, E increases for $v_{inj} > 0$ while in the recirculation zone, E reaches a maximum just near the inlet, and has a minimum at the point of reattachment. The opposite behavior is found for suction. As expected, the calculated von Kármán constant E reaches its nonblowing value of 9.0 for small blowing velocities. For an injection velocity of 0.05 m/s, it was not possible to calculate the von Kármán constant E at every

Table 2 Inlet conditions used in the combustion calculations

$D = 0.20$ m	$T_w = 1100$ K
$h = 0.05$ m	$Y_{O_2} = 0.21$ (O_2/N_2 mixture)
$L = 0.75$ m	$Y_{N_2} = 0.79$
$u_{in} = 30$ m/s	$Y_{O_2} = 0.230$ (air)
$Re_h = 72{,}000$	$Y_{N_2} = 0.755$
$p_{in} = 10^6$ N/m^2	$Y_{Ar} = 0.015$
$T_{in} = 1100$ K	

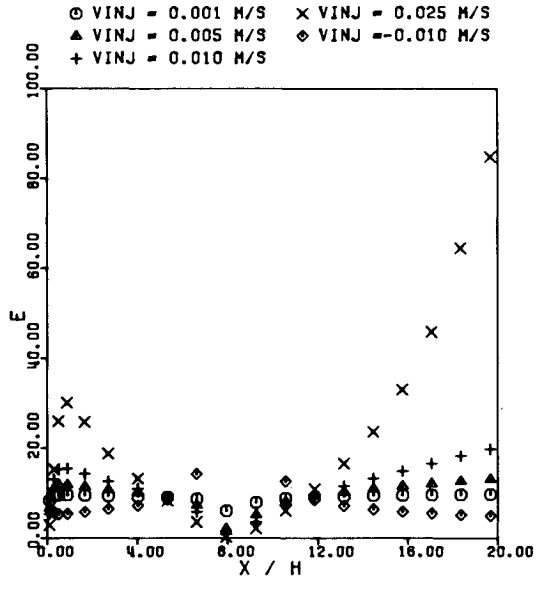

Fig. 3 Variation of the von Kármán constant E with the blowing velocity and the location in the flow.

Table 3 Reactions in consideration

	B	α	E^a		B	α	E^a
$O_2 + H = O + OH$	0.220E12	0.00	0.845E4	$O + O + Ar = O_2 + Ar$	0.191E8	0.00	−0.901E3
$H_2 + O = H + HO$	0.180E8	1.00	0.448E4	$N_2 + O = NO + N$	0.140E12	0.00	0.379E5
$H_2 + OH = H_2O + H$	0.220E11	0.00	0.259E4	$N + O_2 = NO + O$	0.640E7	1.00	0.315E4
$2OH = H_2O + O$	0.630E10	0.00	0.550E3	$O + N_2O = 2NO$	0.100E11	0.00	0.141E5
$H_2 + O_2 = 2OH$	0.251E10	0.00	0.196E5	$N_2 + O_2 = 2NO$	0.212E22	−2.50	0.642E5
$H + HO_2 = 2OH$	0.251E10	0.00	0.956E3	$N_2 + O_2 = N_2O + O$	0.630E11	0.00	0.552E5
$H + HO_2 = H_2 + O_2$	0.250E11	0.00	0.350E3	$N_2 + O_2 = N + NO_2$	0.270E12	−1.00	0.606E5
$H + HO_2 = H_2O + O$	0.500E11	0.00	0.500E3	$H + NO_2 = NO + OH$	0.350E12	0.00	0.740E5
$2HO_2 = H_2O_2 + O_2$	0.200E10	0.00	0.000	$N_2 + OH = N_2O + H$	0.320E10	0.00	0.404E5
$H_2O_2 + OH = HO_2 + H_2O$	0.102E11	0.00	0.910E3	$NO + HO_2 = NO_2 + OH$	0.120E11	0.00	0.198E4
$H_2O_2 + H = H_2 + HO_2$	0.169E10	0.00	0.190E4	$N + OH = H + NO$	0.400E11	0.00	0.000
$H_2O_2 + H = H_2O + OH$	0.318E12	0.00	0.450E4	$NO + O_2 = NO_2 + O$	0.170E10	0.00	0.234E5
$H_2O_2 + O = HO_2 + OH$	0.843E9	0.00	0.213E4	$N + NO_2 = 2NO$	0.360E10	0.00	0.000
$HO_2 + OH = H_2O + O_2$	0.501E11	0.00	0.503E3	$2NO_2 = 2NO + O_2$	0.200E10	0.00	0.135E5
$O + HO_2 = O_2 + OH$	0.501E11	0.00	0.503E3	$N + NO_2 = N_2O + O$	0.500E10	0.00	0.000
$HO_2 + H_2 = OH + H_2O$	0.723E9	0.00	0.941E4	$N + N_2O = NO + N_2$	0.500E6	0.00	0.500E4
$H_2O_2 + O = H_2O + O_2$	0.843E6	0.00	0.212E4	$NO + NO_2 = N_2O + O_2$	0.100E10	0.00	0.302E5
$2H + Ar = H_2 + Ar$	0.640E12	−1.00	0.000	$NO + N_2O = NO_2 + N_2$	0.200E12	0.00	0.250E5
$H + OH + Ar = H_2O + Ar$	0.840E16	−2.00	0.000	$N_2O + OH = N_2 + HO_2$	0.320E11	0.00	0.755E4
$H + O_2 + Ar = HO_2 + Ar$	0.150E10	0.00	−0.500E3	$N + O + Ar = NO + Ar$	0.640E11	−0.5	0.000
$2OH + Ar = H_2O_2 + Ar$	0.907E9	0.00	−0.255E4	$O + NO + Ar = NO_2 + Ar$	0.110E10	0.00	−0.940E3
$H + O + Ar = OH + Ar$	0.100E11	0.00	0.000	$N_2 + O + Ar = N_2O + Ar$	0.140E8	0.00	0.104E5
$O + OH + Ar = HO_2 + Ar$	0.100E12	0.00	0.000	$2N + Ar = N_2 + Ar$	0.300E9	0.00	−0.500E3

[a] $k_f = BT^\alpha \exp(-E/T)$, kmol-m^3-s units.

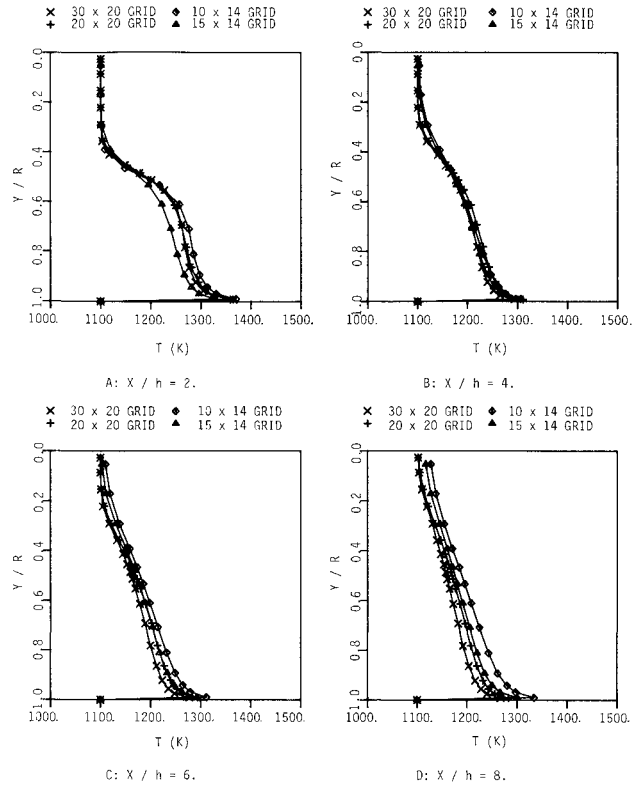

Fig. 4 Temperature profiles for different grid systems.

location in the flow. Furthermore, it was observed that the wall shear stress was acting in the same direction as the velocity parallel to the wall, which is caused by the dominating influence of the second term in Eq. (18) at this blowing velocity. It is therefore believed that for $v_{inj} = 0.05$ m/s, the adapted wall-function method does not hold anymore. Other calculations showed that it is not the value of the blowing velocity, but the ratio of inlet velocity and blowing velocity in combination with the kind of gas injected at the wall, which determines the range of applicability of the adapted wall-function method. Experimental data for flows with blowing or suction available in the literature are concerned with boundary-layer flows over a flat plate, and these data are difficult to compare with the computational results described.

To test the combustion model, the flow and combustion of O_2/N_2 mixtures and air, with H_2 injected at the wall was calculated. Calculations were carried out on a Cray-1S computer. Central processor times varied between 4 and 15 min, depending on the number of gridpoints, species, and reactions taken into account. The inlet conditions are given in Table 2. The number of reactions considered was equal to 24 for the combustion of O_2/N_2 with H_2, and 46 for the combustion of air with H_2. In the latter case, the formation of nitrogen oxides was taken into account. The reactions and their Arrhenius coefficients are given in Table 3.[12] The symbol of species argon in this table is used to indicate three-body recombination reactions.

Calculations were performed studying the effect of the number of gridpoints, blowing velocity at the wall, the expansion ratio, and studying the effect of NO_x formation on the calculation results. Using four different grid systems, Fig. 4 shows the calculated temperature profiles at four different x locations for a flow with H_2 injected at 0.01 m/s. As can be seen from this figure, the results obtained using a 10×14 and 15×14 grid system differ much from the results obtained with the 20×20 and 30×20 grid system, indicating that these first two grid systems are too coarse to obtain an accurate solution. The results obtained with the 20×20 and 30×20 grid are almost equal, indicating that the 20×20 grid system is sufficiently accurate. Because the amount of H_2 injected in the flow is small, it is completely burnt as soon as it enters the flow. Temperature maxima are therefore located just near the wall.

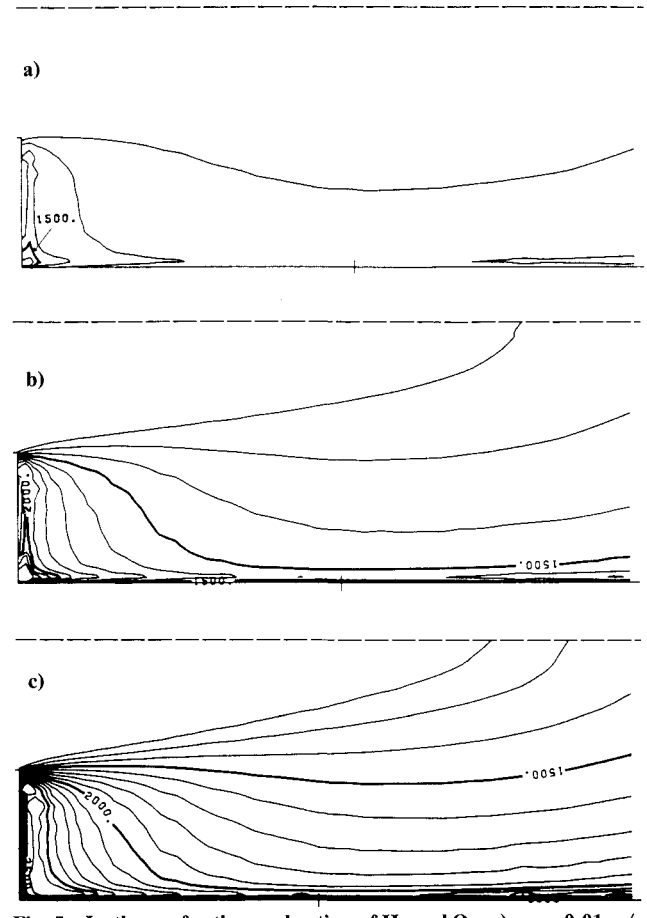

Fig. 5 Isotherms for the combustion of H_2 and O_2: a) $v_{inj} = 0.01$ m/s, b) $v_{inj} = 0.025$ m/s, c) $v_{inj} = 0.05$ m/s.

Figure 5 shows the isotherms of calculations carried out for three blowing velocities at the wall. The overall oxidizer/fuel ratio, defined as

$$O/F = (\rho u Y_{O_2} A)_{in}/(\rho v \pi D L)_w \tag{30}$$

was equal to 150, 60, and 30 for these blowing velocities. It may be seen from Fig. 5 that the highest temperatures occur in the recirculation region just near the inlet of the channel. Increasing the amount of H_2 injected into the flow moves this maximum temperature from the wall in the direction of the centerline, because near the wall the hydrogen is not completely burnt at high blowing velocities. The value of the maximum temperature is hardly affected when doubling the amount of H_2 blown into the flow (compare Figs. 5b and 5c). Maximum temperatures are found in regions where both the H_2 and O_2 are almost completely burnt. Increasing the amount of H_2 blown into the flow increases the size of the fuel rich zone near the wall, resulting in a shift of the location of maximum temperatures from the wall in the direction of the centerline. Comparing the maximum temperatures obtained with the finite chemical kinetics model to the maximum temperatures obtained with a combustion model which considers only one irreversible infinitely fast reaction (diffusion flame model), shows that, in the latter case, maximum temperatures are 125–175 K higher.[13] This difference is caused by the instability of the diffusion flame model to take into account dissociation of species, which is important at high temperatures.

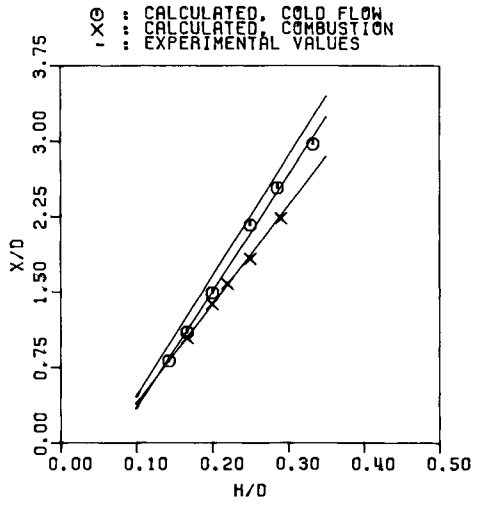

Fig. 6 Reattachment length as function of the step height diameter ratio.

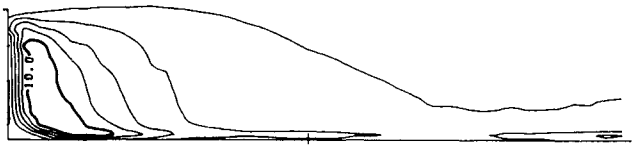

Fig. 7 NO mass fraction distribution X1000 for the combustion of H_2 with air, $v_{inj} = 0.05$ m/s.

Calculations were performed to study the effect of the expansion ratio on the reattachment length. The step height was kept constant, while the channel diameter was varied between 0.175 and 0.30 m. The blowing velocity was equal to 0.05 m/s. Figure 6 shows the calculated reattachment length as function of the step height diameter ratio, calculated with and without combustion, together with experimental results reported by Schulte.[14] A linear regression on the calculated results yielded the following relations between the reattachment length and step height diameter ratio:

$$x_r/D = 9.84(h/D) - 0.60 \qquad c = 0.9990$$

for the calculation with combustion, and

$$x_r/D = 11.73(h/D) - 0.87 \qquad c = 0.9995$$

for the calculation without combustion. In both cases, the correlation coefficient c is close to 1. From Fig. 6 it may be seen that combustion affects the reattachment length. Furthermore, it may be seen that the calculated reattachment lengths with combustion are smaller than the experimental results. The O/F ratio for the combustion calculations is not kept constant, but this seems to have no effect on the linear relation between the reattachment length and the expansion ratio.

Calculations including the formation of NO_x show that in the high-temperature regions of the recirculation zone NO appears, see Fig. 7. Further downstream, the amount of NO_x in the flow is small. Accounting for NO_x formation results in temperatures which are ~30 K lower in the high-temperature region compared with results obtained without taking into account NO_x formation.

Conclusions

The COPPEF computer program was extended to account for heat and mass transfer at the boundaries. The wall-function method of Chieng and Launder was adapted to allow for the calculation of the von Kármán constant E. For relatively small blowing velocities, the adapted wall-function method worked satisfactorily.

A finite-rate chemical kinetics combustion model was implemented in COPPEF. The proposed splitting of the transport equation of mass fractions into a convective/diffusive part, and a chemical production/destruction part, and solving these two parts separately with different techniques, gave good results.

Calculations were carried out simulating the flow and combustion of an O_2/N_2 mixture or air with H_2 injected at the wall. The calculated results for different blowing velocities at the wall were in agreement with what was anticipated. An increase of the amount of injected H_2 results in higher temperatures, and a shift of the location of maximum temperature from the wall. Calculations carried out for different expansion ratios showed that the location of the point of reattachment is a linear function of the expansion ratio.

Taking into account the formation of NO_x resulted in a temperature reduction of maximal 30 K.

Acknowledgments

This work was sponsored by the Technology Foundation (STW), the Project Management Office for Energy Research (PEO), and the Netherlands Organization for the Advancement of Pure Research (ZWO).

References

[1]Korting, P. A. O. G., Geld, C. M. W. van der, Vos, J. B., Wijchers, T., Schöyer, H.F.R., and Nina, M.N.R., "Combustion Behavior of PMMA in a Solid Fuel Ramjet," AIAA Paper 86-1401, June 1986.

[2]Vos, J. B. and Dijk, J. H. van, "The Development of a Computational Model for a 2 Dimensional Turbulent Flow. Part II: Description of the Computer Code and Computational Results of Various Pipe Flows," Dept. of Aerospace Engineering, Delft Univ. of Technology/Prins Maurits Lab. TNO, Rept. LR-469/PML 1985-C22, Delft/Rijswijk, the Netherlands, 1985.

[3]Bredshaw, P., Cebeci, T., and Whitelaw, J. H., *Engineering Calculation Methods for Turbulent Flows*, Academic Press, New York, 1981.

[4]Chieng, C. C. and Launder, B. E., "On the Calculation of Turbulent Heat Transport Downstream from an Abrupt Pipe Expansion," *Numerical Heat Transfer*, Vol. 3, 1980, pp. 189-207.

[5]Jayatilleke, C. L., "The Influence of Prandtl Number and Surface Roughness on the Resistance of the Laminar Sub-Layer to Momentum and Heat Transfer," *Progress in Heat and Mass Transfer*, Vol. 1, 1969, pp. 193-329.

[6]Patankar, S. V. and Spalding, D. B., *Heat and Mass Transfer in Boundary Layers*, 2nd ed., Intertext Books, London, 1970.

[7]Jones, W. P., "Models for Turbulent Flows with Variable Density and Combustion," *Prediction Methods for Turbulent Flows*, edited by W. Kollmann, Hemisphere, Washington 1980.

[8]Vos, J. B., "Combustion Modeling in an SFCC and a Description of the KINETICS-Computer Code," Dept. of Aerospace Engineering, Delft Univ. of Technology/Prins Maurits Lab. TNO, Rept. LR-481/PML 1986-C14, Delft/Rijswijk, the Netherlands, Dec. 1985.

[9]Patankar, S. V., *Numerical Heat Transfer and Fluid Flow*, Hemisphere, Washington, 1980.

[10]Settari, A. and Aziz, K., "A Generalization of the Additive Correction Methods for the Iterative Solution of Matrix Equations," *SIAM Journal of Numerical Analyses*, Vol. 10, No. 3, 1973, pp. 506-521.

[11]Gear, C. W., *Numerical Initial Value Problems in Ordinary Differential Equations*, Prentice-Hall, Englewood Cliffs, NJ, 1971.

[12]Westley, F., "Table of Recommended Rate Constants for Chemical Reactions Occuring in Combustion," NSRDS-NBS 67, U.S. Dept. of Commerical National Bureau of Standards, Washington, DC, 1980.

[13]Elands, P.J.M., "Implementation of a Diffusion Flame Model and a Turbulent Diffusion Flame Model in the COPPEF Computer Program," Faculty of Aerospace Engineering, Delft Univ. of Technology/Prins Maurits Lab. TNO, Rept. LR-494/PML 1986-C65, Delft/Rijswijk, the Netherlands, 1986.

[14]Schulte, G., "Fuel Regression and Flame Stabilization Studies of Solid-Fuel Ramjets," *Journal of Propulsion and Power*, Vol. 2, July-Aug. 1986, pp. 301-304.